Defect analysis of 1-MeV electron irradiated flexible InGaAs solar cells by deep-level transient spectroscopy and photoluminescence

Z.X. Wang [a], M.Q. Liu [b], T.B. Wang [a], S.Y. Zhang [a], M. Li [a], G.H. Tang [a], Y. Zhuang [a], X. Yang [a], L. Zhong [b],[**], A. Aierken [a],[*]

[a] *School of Energy and Environment Science, Yunnan Normal University, 650500, Kunming, China*
[b] *Institute of Electronic Engineering, China Academy of Engineering Physics, Mianyang, 621900, China*

A B S T R A C T

1-MeV electron irradiated InGaAs flexible solar cells were investigated based on solar cell I–V characteristics, external quantum efficiency, photoluminescence, and deep-level transient spectra (DLTS) mesurements. The electrical parameters of the solar cells, including R_s and R_{sh}, were extracted from the I–V curves. With an increase in irradiation fluence, the electrical and optical characteristics of the solar cells continuously degraded. The V_{oc}, I_{sc}, and P_{max} values decreased to 83.16%, 81.96%, and 68.88% of their initial values, respectively, when the irradiation fluence was increased to 2×10^{15} e/cm^2. Photoluminescence (PL) emission peak intensity decreased to 0.54% of its original value, and the minority carrier lifetimes derived from fitting PL emission spectra were reduced to 1.25%. DLTS technique was used to analyse the irradiation-induced defect properties. Similar fitting values for the minority carrier lifetimes were obtained from the PL and DLTS measurements.

1. Introduction

Inverted metamorphic (IMM) GaAs multijunction solar cells enable current matching between their subcells and have significant space-application potential [1]. With the continuous development of epitaxial technology, flexible solar cell devices have shown superior performance as compared with traditional rigid devices in space applications, including a low weight, high flexibility, and high power ratio [2]. Flexible four-junction (4J) AlGaInP/AlGaAs/In$_{0.17}$Ga$_{0.83}$As/In$_{0.47}$Ga$_{0.53}$As IMM solar cells were reported by Huang et al., exhibiting a 25.76% efficiency under AM 1.5 G [3]. To prevent the negative effects of Zn diffusion in the back surface field layer, Wang et al. fabricated flexible IMM GaInP/GaAs/InGaAs triple-junction solar cells using a C source for p-type doping and obtained a 34.52% efficiency under AM 1.5 D [4]. Sharp reported a flexible IMM 3J solar cell with a conversion efficiency of 37.5% (AM 1.5 G) [5]. With their distinct benefits and potential, flexible IMM solar cells are quickly outperforming other space solar cell types as industry standards.

Because the solar cell arrays of in-orbit spacecraft suffer from high-energy particle irradiation such as that from electrons and protons, conducting on-ground irradiation experiments to investigate radiation

damage and to optimise cell structures to improve the radiation resistance of spacecraft is crucial. Degraded cell performance is significantly affected by the energy level, concentration, and capture cross section of solar cell crystal defects. Multiple investigations have demonstrated that particles with different energies create nonradiative traps in the bandgaps of GaInP, GaAs, and InGaAs solar cells under various fluences [6–8]. Deep-level transient spectrum (DLTS) and electroluminescence techniques have been used to study 1.8-MeV electron irradiated GaInP cells, and H2 (E$_v$+0.55 eV) has been determined to be a nonradiative recombination centre that affects the minority carrier lifetime [9]. After exposure to 150-KeV proton radiation, GaAs cells were subjected to defect analysis. Photoluminescence technology was also used to measure the nonradiative minority lifetimes of the GaAs cells under various radiation doses. Through a COMSOL simulation, the EL2 defect (E$_v$+0.71 eV) agreed with the experimental data [10]. The nonradiative recombination centers of GaInP cells after 3-MeV proton irradiation were confirmed to be electron traps E5 (E$_c$-0.96 eV) and hole traps H2 (E$_v$+0.55 eV) [11]. Hole trap H0 (E$_v$+0.09 eV) appeared in the InGaAs (1.0 eV) subcell, H1 (E$_v$+0.07 eV), H2 (E$_v$+0.30 eV), and H3 (E$_v$+0.45 eV) appeared in the InGaAs (0.7 eV) solar cells irradiated by 5-MeV proton, and H2 and H3 were determined by density functional theory

---

* Corresponding author.
** Corresponding author.
E-mail addresses: zhongle_mtrc@caep.cn (L. Zhong), erkin@ynnu.edu.cn (A. Aierken).

to be $V_{Ga\ (0/-1)}$ and $V_{Ga\ (-1/-2)}$ or possibly $V_{As\ (+3/+1)}$ [12]. Zhang et al. studied IMM 4J GaInP(1.89 eV)/GaAs(1.4 eV)/In$_{0.3}$Ga$_{0.7}$As(1.0 eV)/In$_{0.58}$Ga$_{0.42}$As(0.7 eV), where an E_c-0.52 eV trap was found in the In$_{0.58}$Ga$_{0.42}$As cell prior to irradiation. It then changed to E_c-0.46 eV and E_c-0.58 eV traps when the irradiation fluence increased. In In$_{0.3}$Ga$_{0.7}$As subcells, an E_c-0.03 eV defect was observed, and defect concentration N_T, energy level E_T, and capture cross-section σ increased with the increase in irradiation fluence [13]. DLTS analysis of the UMM 4J AlGaInP (1.89 eV)/AlInGaAs(1.45 eV)/InGaAs (1.14 eV)/Ge(0.67 eV) was performed, and DLTS measurements determined that the concentration of the original defects and irradiation-induced defects in the three subcells increased with an increase in irradiation fluence [14]. Xu et al. investigated IMM 3J GaInP/GaAs/InGaAs solar cells irradiated by 2-MeV protons under the electroluminescence (EL) method and showed a nonradiative recombination centre caused by irradiation [15].

However, few investigations have been conducted on the irradiation effects of flexible IMM 3J solar cells. Since the InGaAs subcell plays an important role in the performance of triple-junction cells before and after irradiation, studying the radiation effects of flexible InGaAs solar cells and its degradation mechanism by radiation induced defects provides a theoretical and experimental data for optimizing high-efficiency radiation hardened flexible IMM 3J solar cells. This study investigated 1-MeV electron irradiation effects on InGaAs single-junction flexible solar cells by combining DLTS technology, electrical and spectral performance testing and fitting, photoluminescence measurements, and Mulassis (Multi-layered shielding simulation software) simulation method.

2. Experiments

InGaAs solar cells were fabricated using a metal-organic vapour phase epitaxy (MOCVD) system via an inverted metamorphic epitaxial growth technique. Details of sample preparation are reported in our previous work [4]. The sample structure is illustrated in Fig. 1, the bandgap of the InGaAs solar cells is 1.0 eV, and all cell devices are 2 × 4 cm² in size.

The irradiation experiment was conducted at the Institute of Space Environment and Physical Science of the Harbin Institute of Technology using a 1-MeV-electron ELV-8II high-voltage accelerator with an irradiation flux of 1×10^{11} cm^{-2}s^{-1} at room temperature. According to space solar cell irradiation test standards [16], the irradiation fluences were selected as 1×10^{14} e/cm², 1×10^{15} e/cm², and 2×10^{15} e/cm². Two separate samples were used for each irradiation dose.

The I–V characteristics of the solar cells were measured using an OAI TSS-156 solar simulator at 25 °C under AM 0 spectrum (136.7 mW/cm²). A SOFN 7-SCSpec111 spectral-response test system was used to measure the external quantum efficiency (EQE) of the solar cells in the spectral window of 800–1400 nm. To further investigate the degradation of cell performance caused by defects, DLTS measurements were conducted using a PhysTech FT 1230 DLTS test system in a 20–400 K temperature range, and defect properties such as the energy level and concentration were extracted from the DLTS spectra. A low-temperature photoluminescence test of the InGaAs epitaxial wafer was performed using a HORIBA QuantaMaster-8000 system, and a 785-nm continuous wavelength laser with a laser power density of 25 mW/cm² was used for excitation. Mulassis simulation software was used to calculate the displacement damage dose (DDD) of 1 MeV electrons in InGaAs single-junction solar cells with different fluences.

## 3. Results and DISCUSSION

3.1. Degradation of electrical performance

Fig. 2 (a) shows the relationship between the 1 MeV electron incidence depth DDD at the irradiation dose of 1×10^{15} e/cm², simulated by MULASSIS software. Displacement damage occurs when particles collided with the lattice atoms, high energy electrons transferring energy to the lattice atoms and generating displacement damage defects, thus affecting the cell performance. According to the non-ionizing energy loss (NIEL) approach, DDD values in solar cell materials can be expressed as [17]:

$$DDD = NIEL \times \varnothing \tag{1}$$

where NIEL is the non-ionizing energy loss value of the solar cell material for the corresponding irradiated particle and its energy, φ is the irradiation dose.

The results show that when the electron incidence depth increased, the DDD produced in the solar cell active layer increases continuously due to the increase of the NIEL value because of the decrease in particle energy due to the collision with the lattice atoms. The average DDD values in InGaAs solar cells under 1×10^{14} e/cm², 1×10^{15} e/cm², and 2×10^{15} e/cm² electron fluence are shown in Fig. 2(b), the DDD values increases with the increase in irradiation fluence.

The changes in the electrical parameters of the flexible single-junction InGaAs solar cells at different irradiation fluences are presented in Table 1. The measured and fitted I–V curves of the InGaAs solar cells before and after 1-MeV electron irradiation are shown in Fig. 3, and the degradation of the normalised I_{sc}, V_{oc}, and P_{max} values are plotted in Fig. 4. Figs. 3 and 4 and Table 1 show that all the electrical parameters of the InGaAs solar cells degraded after irradiation. When the irradiation dose increased to 2×10^{15} e/cm², V_{oc}, I_{sc}, and P_{max} all degraded to 83.16%, 81.96%, and 68.88% of their initial values, respectively.
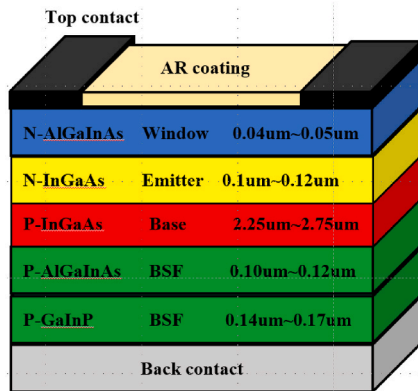
(a)
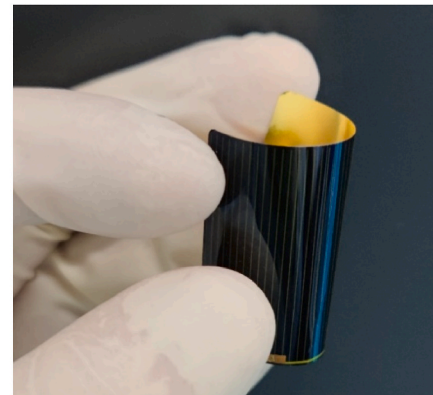
(b)

Fig. 1. (a) Structure of a flexible IMM single-junction InGaAs (b) solar cell device.
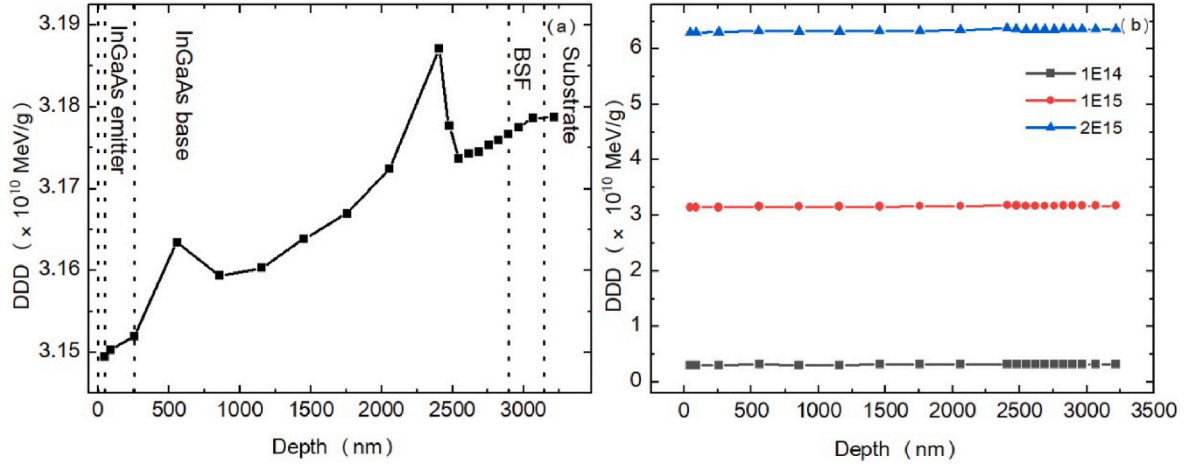
Fig. 2. The *DDD* of InGaAs solar cells (a), and average *DDD* values under different irradiance fluences(b).

Table 1
Changes in I_{sc}, V_{oc}, and P_{max} values of 1-MeV electron irradiated InGaAs solar cells.

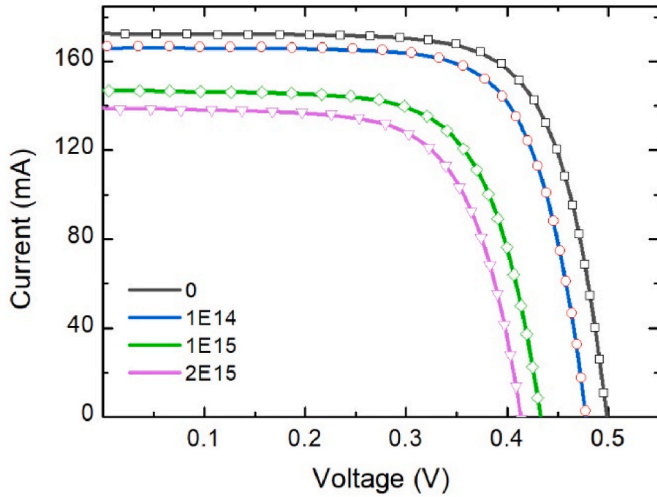| Fluence (cm^{-2})	I_{sc} (mA)	V_{oc} (V)	FF (%)	E_{ff} (%)	P_{max}(mW)
0	168.99	0.493	78.20	6.02	65.17
1×10^{14}	164.11	0.478	79.48	5.77	62.44
1×10^{15}	146.56	0.431	79.68	4.65	50.38
2×10^{15}	138.51	0.410	78.86	4.15	44.89

Fig. 3. InGaAs solar cell I–V curves before and after 1-MeV electron irradiation, where solid lines and symbols indicate the measured and fitted values, respectively.

Significant degradation began when the fluence was increased to 1×10^{15} e/cm^2, and further degradation occurred when the irradiation fluence was further increased to 2×10^{15} e/cm^2.

The single-junction solar cell current–voltage relationship can be expressed as [18]:

$$I = I_{ph} - I_0 \left[\exp\left(\frac{V + IR_S}{nkT} \right) - 1 \right] - \frac{V + IR_s}{R_{sh}} \qquad (2)$$

Table 2 listed the fitting results of the solar cell electrical parameters, including the photogenerated current I_{ph}, dark current I_0, ideal factor n, series resistance R_s, and parallel resistance R_{sh} before and after irradiation. Table 2 shows that I_{ph} and R_{sh} decreased as the irradiation fluence
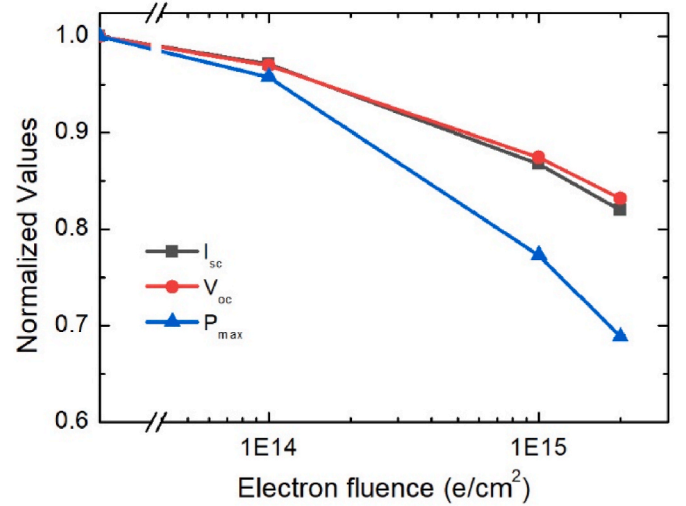

Fig. 4. Degradation of InGaAs solar cell electrical parameters at various levels of 1-MeV electron fluence irradiation.

Table 2
Fitted electrical parameters of 1-MeV electron irradiated InGaAs solar cells.

Fluence (e/cm^{-2})	I_{ph}(mA)	I_0(A)	N	R_s(Ω)	R_{sh}(Ω)
0	172.5	3.40E-07	1.45	0.031	400
1×10^{14}	166.9	5.09E-07	1.45	0.044	314
1×10^{15}	146.9	2.18E-06	1.50	0.059	214
2×10^{15}	138.9	3.37E-06	1.51	0.060	191

increased, whereas I_0 and R_s increased with an increase in irradiation fluence.

The displacement damage defects created by irradiation in the solar cell active region create non-radiative recombination centers [19] and decreases the diffusion length and collection efficiency of photo-generated minority carriers, and, this is the primary cause of I_{ph} degradation in the ideal solar cell equivalent circuit model. The relationship between the minority carrier diffusion length and the electron irradiation fluence can be expressed as below [20]:

$$\frac{1}{L_\emptyset 2} = \frac{1}{L_0 2} + K_L \emptyset \qquad (3)$$

where K_L is the diffusion length damage coefficient, and $L_\emptyset$, L_0 is the diffusion length of the minority carriers before and after irradiation.

Additionally, the minority carrier lifetime (τ) and the diffusion length (L) are depend each other by the relationship of $L = \sqrt{D\tau}$. As the irradiation fluence increased, the defect concentration increased in the cell materials, the minority carrier lifetime decreased, and the diffusion length shortened. Furthermore, displacement damage leads to the carrier removal effect, which lowers the concentration of the majority carriers in the emission region and base region and has an impact on the built-in electric field V_D.

$$V_D \approx \frac{K_B T}{q} \ln \left(\frac{n_{n0} p_{p0}}{n_i^2} \right) \tag{4}$$

where n_{n0} and p_{p0} are the majority carrier concentrations in the emission region and base region, respectively, and n_i^2 is the intrinsic carrier concentration. K_B is the Boltzmann constant. When the concentration of the majority carriers deceases, the internal electric field V_D became weaker, and, consequently, the collecting efficiency photogenerated carriers decreases and the R_s of the solar cell increases after the carrier removal impact. Furthermore, V_{oc} and I_0 can be expressed as [21,22]:

$$V_{oc} = n \frac{K_B T}{q} \ln \left(\frac{I_{ph}}{I_0} + 1 \right) \tag{5}$$

$$I_0 \propto J_S = \frac{q D_n n_{p0}}{L_n} + \frac{q D_p p_{n0}}{L_p} \tag{6}$$

where L_n is the electron diffusion length in the p-type base area, L_p is the hole diffusion length in the n-type emission region, and J_S is the reverse saturation current density, which is proportional to I_0. The minority carrier concentration in the condition of non-illuminated thermal equilibrium is represented by n_{p0}, n_{n0}, and $D_{n,p}$ are the diffusion coefficients of minority electrons (p-type region) and minority holes (n-type region), respectively. When high-energy particles induce defects in the junction area, deep energy levels are created in the band gap, which serves as the recombination centers and traps. At the same time, solar cell leakage current increases and resulting in the reduction of the parallel resistance R_{sh} and the degradation of V_{oc} [23,24]. By fitting the I–V curves of the solar cells corresponding to each irradiation fluence, we were able to extract these electrical parameters (Table 2), and the results were consistent with the changes in the main electrical parameters of the solar cells (Table 1).

3.2. Degradation of spectral performance

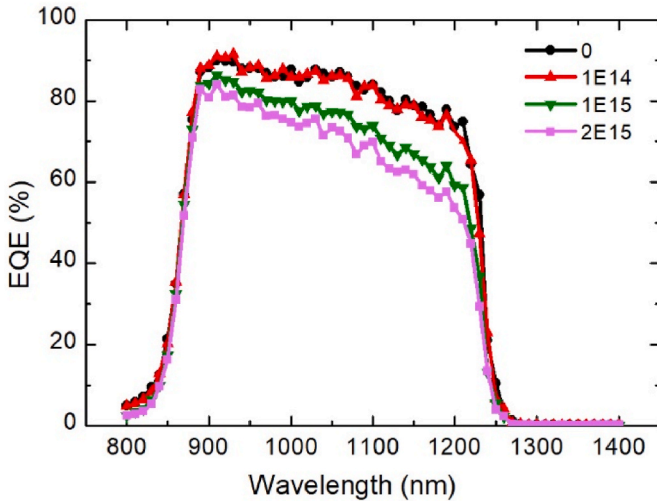Fig. 5 shows the EQE spectra of the InGaAs solar cells at various fluences of 1-MeV electron irradiation. The results showed that the EQE values decreased significantly with increasing irradiation fluence up to 1×10^{15} e/cm^2 and decreased even more when the electron fluence reached 2×10^{15} e/cm^2. The degradation of EQE in the long-wave region is larger than that in the short-wave region. There are two reasons for this, firstly, it can be seen from Fig. 2 that *DDD* values increases with the increase of electron beam incidence depth and results in higher *DDD* in solar cell base region than that of in the emitter layer. Secondly, since the base regions is much thicker than the emission region and had a higher probability of capturing photogenerated carriers than the emission and depletion regions, therefore, quantum efficiency of solar cell degraded in the long-wave region was more severe [25].

Fig. 6 shows the low-temperature (10 K) normalised PL curves of the InGaAs single-junction solar cells exposed to different irradiation fluences of 1-MeV electron. The emission peak of InGaAs was observed at 1260 nm (0.98 eV), and the peak intensity decreased sharply with increasing irradiation fluence. As the irradiation fluence increased to 1×10^{14} e/cm^2, 1×10^{15} e/cm^2, and 2×10^{15} e/cm^2, the PL intensity decreased to 20.3%, 3.7%, and 0.54% of its initial value, respectively. The decrease of PL intensity indicates the increase of non-radiative recombination, which leads to the increase of electron-hole pair recombination rate, resulting in the decrease of short circuit current and radiation efficiency η [26].

Under certain excitation conditions, the radiation efficiency η can be derived from the PL intensity and expressed as [27]:

$$\eta = \frac{1}{\left(1 + \frac{\tau r}{\tau nr} \right)} \tag{7}$$

Where τ_r is the radiative recombination lifetime and τ_{nr} is the nonradiative recombination lifetime of minority carriers. The radiation recombination lifetime τ_r is expressed as $\tau_r = 1/BN$, and the nonradiative recombination lifetime τ_{nr} is expressed as $\tau_{nr} = 1/k\sigma\upsilon\varphi$. Therefore, equation (7) became to:

$$\eta = \frac{1}{\left(1 + \frac{k\sigma\upsilon}{BN}\varnothing \right)} \tag{8}$$

where B is the radiation recombination probability [28], k is the introduction rate of the nonradiative recombination centre, σ is the capture cross section of the minority carriers, υ is the carrier thermal velocity, and N is the doping concentration.

Fig. 5. EQE spectra of InGaAs single-junction solar cells exposed to various fluences of 1-MeV electron irradiation.
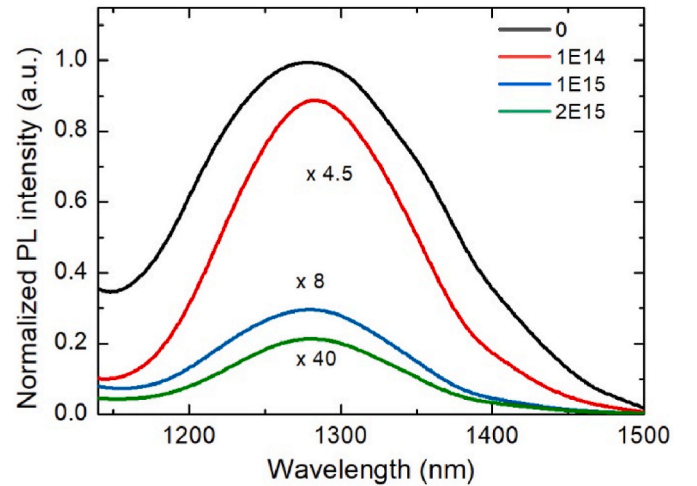

Fig. 6. Low-temperature (10 K) normalised PL curves of InGaAs single-junction solar cells exposed to 1-MeV electrons at various fluences.

$$B = 0.58 \times 10^{-12} \sqrt{\varepsilon} \left(\frac{1}{m_p + m_n} \right)^{1.5} \times \left(1 + \frac{1}{m_p} + \frac{1}{m_n} \right) \left(\frac{300}{T} \right)^{1.5} E_g^2 \quad (9)$$

where E_g, ε, m_n and m_p are the material's band gap, dielectric constant, electron effective mass, and proton effective mass, respectively. It is clear that the radiation recombination probability B has nothing to do with the amount of radiation fluence but is dependent of the electron effective mass, the proton effective mass, the dielectric constant, and the band gap. As a result, its value is unaffected by radiation exposure. $B = 2.0 \times 10^{-10}$ cm^3/s can be obtained by adding the respective parameter values [29].

It should be noted that the η is inversely proportional to the irradiation fluence φ. When the solar cells are irradiated with φ, it creates significant numbers of nonradiative recombination centers in solar cell materials and reduces the radiation efficiency and lowers the PL intensity [30,31].

Therefore, Eq. (8) can be rewritten as $\eta = (1 + \alpha\varphi)^{-1}$, where $\alpha = k\sigma\nu/BN$ [32]. The PL-normalised spectra of the InGaAs solar cells as shown in Fig. 6 were fitted using this result, and the fitting curve is shown in Fig. 7.

The effective minority lifetime τ_{eff} can be expressed as [32].

$$\frac{1}{\tau_{eff}} = \frac{1}{\tau_r} + \frac{1}{\tau_{nr}} \quad (10)$$

The radiative recombination lifetime τ_r remained unchanged before and after irradiation. Therefore, the effective minority lifetimes before and after irradiation were calculated by Eq. (10) and the results are listed in Table 3. The effective minority lifetime of 1-MeV electron irradiated InGaAs solar cell decreased continuously as the irradiation fluence is increased.

3.3. DLTS analysis

Fig. 8 shows the DLTS measurement results of the InGaAs solar cells irradiated under different electron fluences in the temperature range of 20–400 K. The InGaAs solar cells are n+/p-type structures. In the DLTS setup, the reverse bias U_R is -6.0V, the filling pulse voltage U_P is 0.01V, the filling pulse width t_p is 0.1 ms, and the cycle T_w is 60.42 ms. The detected DLTS peaks are shown as hole traps, and their defect characteristics are showed in Fig. 8.

The adverse effects of these defects on the minority carrier lifetime of solar cells were analysed. Based on the defect properties, the minority carrier lifetime τ can be expressed as
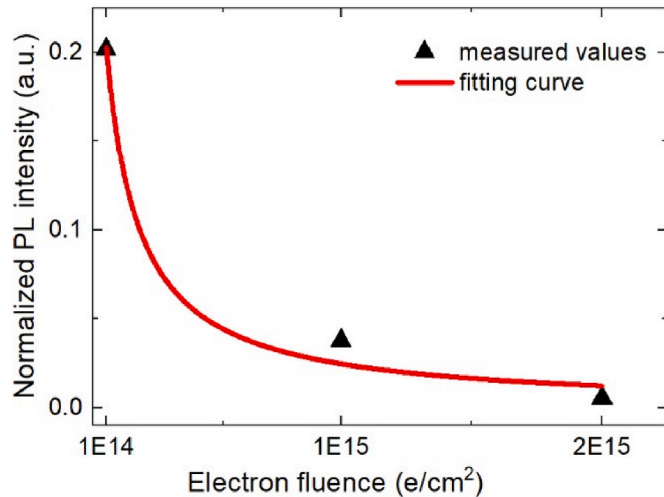

Fig. 7. Changes in InGaAs solar cell PL peak intensity after electron irradiation and corresponding fitting curve.

Table 3
Changes of τ in InGaAs solar cells under different irradiation fluences.

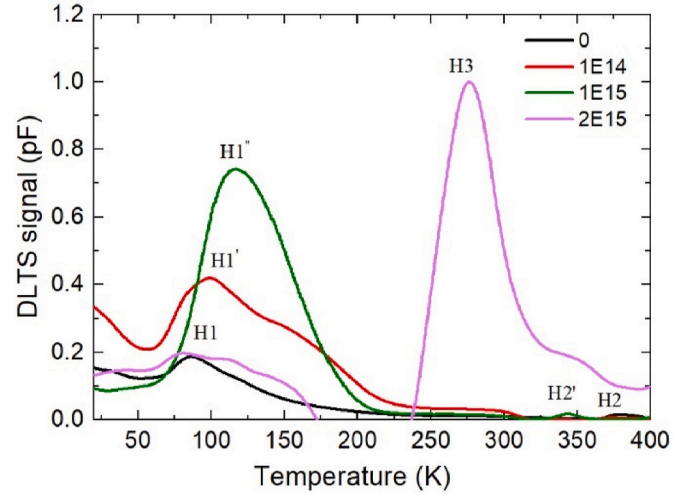|	Fluence (cm^{-2})	B (cm^3/s)	N (cm^{-3})	α	kσν	τ (s)
InGaAs	0	2.0×10^{-10}	1.0×10^{17}	3.93×10^{-14}	5.62×10^{-7}	5.00×10^{-8}
	1×10^{14}					1.01×10^{-8}
	1×10^{15}					1.24×10^{-9}
	2×10^{15}					6.28×10^{-10}

Fig. 8. DLTS curves of 1-MeV-electron-irradiated InGaAs solar cells under different fluences.

$$\frac{1}{\tau_{eff}} = \frac{1}{\tau_r} + N_t \sigma \nu_{th} \quad (11)$$

where N_t is the defect concentration in cm^{-3}, σ is the defect capture cross section in cm^2, and ν_{th} is the carrier thermal motion rate in cm/s. The carrier thermal motion rate and defect capture cross section of the InGaAs solar cell were selected as 4.54×10^7 cm/s and 1.0×10^{-14} cm^2 [33]. The minority carrier lifetimes of the InGaAs solar cells as calculated according to (11) under different irradiation fluences are listed in Table 4.

The non-irradiated InGaAs solar cells exhibited two initial peaks, namely, hole defects H1 (E$_c$-0.141 eV) and H2 (E$_c$-0.727 eV), and the principal defect energy level affecting the cell performance was H1 (according to Figs. 7 and 8 and Table 4). Defect H1 changed to H1' (E$_c$-0.169 eV) as the electron fluence reached 1×10^{14} e/cm^2, and the defect concentration increased. H1' (E$_c$-0.169 eV) was the principal defect energy level that caused the cell performance to decline with irradiation. In addition, H2 (E$_c$-0.727 eV) disappeared and H3 (E$_c$-0.521 eV)

Table 4
Deep-energy-level defect characteristic values of 1-MeV-electron-irradiated InGaAs subcells measured under various irradiation fluences.

Fluence (cm^{-2})	Defect	E$_c$-E$_t$ (eV)	N$_t$ (cm^{-3})	τ(s)
0	H1	0.141	6.56×10^{13}	2.01×10^{-8}
	H2	0.727	5.18×10^{12}	4.47×10^{-8}
1×10^{14}	H1'	0.169	2.13×10^{14}	8.57×10^{-9}
	H3	0.521	1.43×10^{13}	3.77×10^{-8}
1×10^{15}	H1''	0.203	3.86×10^{14}	5.12×10^{-9}
	H2'	0.653	9.66×10^{12}	4.10×10^{-8}
2×10^{15}	H1	0.136	1.51×10^{14}	1.13×10^{-8}
	H3	0.521	9.58×10^{14}	3.45×10^{-9}

appeared with an increase in the shallow energy level and defect concentration. Shallow-energy-level peak H1′ changed to deep-energy-level peak H1′′ when the electron fluence increased to 1×10^{15} e/cm² with a higher defect concentration. Deep-energy-level H2′ appeared, and the concentration decreased as compared with that of H3 under 1×10^{14} e/cm² irradiation. This indicated that the defect concentration of shallow-energy-level defects generated by irradiation increased with increasing irradiation fluence, which resulted in a reduction in the minority carrier lifetime. It was assumed that the shallow energy level H1′′ defect severely hindered cell performance. The concentration of shallow-energy-level H1 (E_c-0.136 eV) decreased when the irradiation fluence reached 2×10^{15} e/cm², whereas deep-energy-level H3 (E_c-0.521 eV) defect concentration increased to its maximum. H3 was determined to be a defect that significantly degraded cell performance. The minority carrier lifetime as derived from DLTS was compared with the PL results, as shown in Fig. 9. Fig. 9 shows that the minority carrier lifetimes derived from DLTS and PL measurements were quite close, and the study showed that the irradiation-induced defects that degraded cell performance were H1, H1′, H1′′, and H3.

4. Conclusion

Through DLTS, PL, I–V characteristics, and EQE, the irradiation damage mechanism of flexible IMM InGaAs solar cells under 1-MeV electron irradiation was investigated. The findings revealed that the electrical and optical properties of InGaAs solar cells degraded significantly with increasing irradiation fluence. When the irradiation fluence was 2×10^{15} e/cm², I_{sc} and P_{max} degraded more than V_{oc}, with P_{max} degrading the most. V_{oc}, I_{sc}, and P_{max} were reduced to 83.16%, 81.96%, and 68.88% of their original values, respectively. The EQE and PL measurement results were also consistent with the degradation trends of the electrical properties of the solar cells with increasing irradiation fluence. As the irradiation fluence increased to 1×10^{14} e/cm², 1×10^{15} e/cm², and 2×10^{15} e/cm², the PL peak intensity of the InGaAs emission peak decreased to 20.3%, 3.7%, and 0.54% of its initial value, respectively, and the fitted values of the minority carrier lifetimes based on PL spectra gradually decreased to 20.2%, 2.48%, and 1.25% of their original values, respectively. The changes in minority carrier lifetimes in solar cells caused by irradiation were investigated by DLTS technology, and the results indicated that minority carrier lifetimes decreased with increasing irradiation fluence, proving that the irradiation-induced defects in H1, H1′, H1′′, and H3 primarily explained cell performance degradation. By fitting the PL and DLTS spectra, we derived similar values and degradation trends of the minority carrier lifetimes with increasing irradiation fluence.

CRediT authorship contribution statement

Z.X. Wang: Writing – original draft, Validation, Software, Methodology, Investigation, Data curation, Conceptualization. **M.Q. Liu:** Writing – original draft, Software, Methodology, Investigation, Formal analysis, Data curation. **T.B. Wang:** Writing – original draft, Validation, Methodology, Investigation. **S.Y. Zhang:** Writing – original draft, Validation, Methodology, Investigation. **M. Li:** Validation, Methodology, Investigation, Conceptualization. **G.H. Tang:** Validation, Methodology, Investigation, Conceptualization. **Y. Zhuang:** Writing – original draft, Validation, Methodology, Investigation. **X. Yang:** Writing – original draft, Validation, Methodology, Investigation. **L. Zhong:** Writing – review & editing, Writing – original draft, Validation, Supervision, Methodology, Data curation, Conceptualization. **A. Aierken:** Writing – review & editing, Writing – original draft, Validation, Supervision, Methodology, Funding acquisition, Data curation, Conceptualization.

Declaration of competing interest

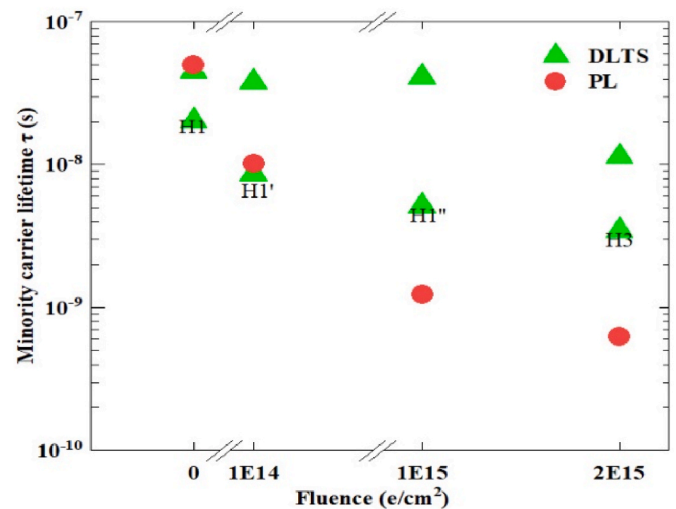The authors declare that they have no known competing financial

Fig. 9. Comparison of minority carrier lifetimes derived from DLTS and PL methods.

interests or personal relationships that could have appeared to influence the work reported in this paper.

References

[1] J.G.J. Adams, V.C. Elarde, G. Hillier, C. Stender, F. Tuminello, A. Wibowo, C. Youtsey, Z. Bittner, S.M. Hubbard, E.B. Clark, M.F. Piszczor, M. Osowski, Improved radiation resistance of epitaxial lift-off inverted metamorphic solar cells, in: 2013 IEEE 39th Photovolt. Spec. Conf. PVSC, IEEE, Tampa, FL, USA, 2013, pp. 3229–3232, https://doi.org/10.1109/PVSC.2013.6745140.

[2] C.L. Stender, J. Adams, V. Elarde, T. Major, H. Miyamoto, M. Osowski, N. Pan, R. Tatavarti, F. Tuminello, A. Wibowo, C. Youtsey, G. Ragunathan, Flexible and lightweight epitaxial lift-off GaAs multi-junction solar cells for portable power and UAV applications, in: 2015 IEEE 42nd Photovolt. Spec. Conf. PVSC, IEEE, New Orleans, LA, 2015, pp. 1–4, https://doi.org/10.1109/PVSC.2015.7356137.

[3] X. Huang, J. Long, D. Wu, S. Ye, X. Li, Q. Sun, Z. Xing, W. Yang, M. Song, Y. Guo, S. Lu, Flexible four-junction inverted metamorphic AlGaInP/AlGaAs/In0.17Ga0.83As/In0.47Ga0.53As solar cell, Sol. Energy Mater. Sol. Cells 208 (2020), 110398, https://doi.org/10.1016/j.solmat.2020.110398.

[4] B. Wang, L. Fang, A. Aierken, Z.G. Tang, W. Du, J.H. He, J.J. Huang, H.L. Huang, W.Y. Yang, K. Chen, J. Li, X. Yang, Y. Zhuang, W.N. Zhang, J.H. Mo, Effects of Zn diffusion in tunnel junction and its solution for high efficiency large area flexible GaInP/GaAs/InGaAs tandem solar cell, Sol. Energy Mater. Sol. Cells 230 (2021), 111257, 10/gnn7js.

[5] K. Sasaki, T. Agui, K. Nakaido, N. Takahashi, R. Onitsuka, T. Takamoto, Development of InGaP/GaAs/InGaAs Inverted Triple Junction Concentrator Solar Cells, Miyazaki, Japan, 2013, pp. 22–25, https://doi.org/10.1063/1.4822190.

[6] A. Khan, M. Yamaguchi, J.C. Bourgoin, T. Takamoto, Thermal annealing study of 1 MeV electron-irradiation-induced defects in n+p InGaP diodes and solar cells, J. Appl. Phys. 91 (2002) 2391–2397, 10/fh52sx.

[7] J. Li, J. Wang, C. Shi, Z. Wang, Y. Xue, Research on the emitter thickness optimization of GaInP/GaAs/Ge triple-junction solar cell under space proton irradiation based on TCAD simulation, AIP Adv. 10 (2020), 115110, https://doi.org/10.1063/5.0029312.

[8] N. Dharmarasu, M. Yamaguchi, J.C. Bourgoin, T. Takamoto, T. Ohshima, H. Itoh, M. Imaizumi, S. Matsuda, Majority- and minority-carrier deep level traps in proton-irradiated n+/p-InGaP space solar cells, Appl. Phys. Lett. 81 (2002) 64–66, 10/cxdfcp.

[9] T. Yi, M. Lu, K. Yang, P. Xiao, R. Wang, Electroluminescence analysis of injection-enhanced annealing of electron irradiation-induced defects in GaInP top cells for triple-junction solar cells, Nucl. Instrum. Methods Phys. Res. Sect. B Beam Interact. Mater. Atoms 335 (2014) 66–69, https://doi.org/10.1016/j.nimb.2014.06.006.

[10] Y. Yan, M. Fang, X. Tang, F. Chen, H. Huang, X. Sun, L. Ji, Effect of 150 keV proton irradiation on the performance of GaAs solar cells, Nucl. Instrum. Methods Phys. Res. Sect. B Beam Interact. Mater. Atoms 451 (2019) 49–54, https://doi.org/10.1016/j.nimb.2019.04.065.

[11] J.L. Wang, T.C. Yi, Y. Zheng, R. Wu, R. Wang, 3.0 MeV proton-irradiation induced non-radiative recombination center in the GaAs middle cell and the GaInP top cell of triple-junction solar cells, IOP Conf. Ser. Earth Environ. Sci. 93 (2017), 012060, https://doi.org/10.1088/1755-1315/93/1/012060.

[12] J. Zhou, Y. Zhang, C. Liu, Y. Jiang, B. Zhou, C. Qi, T. Wang, G. Ma, L. Xiao, M. Huo, Effects of proton radiation on the InGaAs component cells of inverted metamorphic four-junction solar cells, Mater. Sci. Semicon. Process. 162 (2023), 107498, https://doi.org/10.1016/j.mssp.2023.107498.

[13] Y. Zhang, C. Qi, T. Wang, G. Ma, H.-S. Tsai, C. Liu, J. Zhou, Y. Wei, H. Li, L. Xiao, Y. Ma, D. Wang, C. Tang, J. Li, Z. Wu, M. Huo, Electron irradiation effects and defects analysis of the inverted metamorphic four-junction solar cells, IEEE J. Photovoltaics 10 (2020) 1712–1720, https://doi.org/10.1109/JPHOTOV.2020.3025442.

[14] Y. Zhang, J. Zhou, C. Liu, C. Qi, T. Wang, G. Ma, B. Zhou, L. Xiao, M. Huo, Electron irradiation effects and defects analysis of the upright metamorphic four-junction (UMM4J) solar cells, Phys. Status Solidi A 219 (2022), 2100704, https://doi.org/10.1002/pssa.202100704.

[15] J. Xu, G. Yan, M. Lu, Evaluation of the minority-carrier lifetime of IMM3J solar cells under proton irradiation based on electroluminescence, Crystals 13 (2023) 297, https://doi.org/10.3390/cryst13020297.

[16] I.S.O. Geneva, International Organization for Standardization, Space Systems—Space Solar Cells — Electron and Proton Irradiation Test Methods, ISO, 2018. https://www.iso.org/standard/69495.html. (Accessed 12 October 2023).

[17] X.F. Zhao, A. Aierken, M. Heini, M. Tan, Y.Y. Wu, S.L. Lu, R.T. Hao, J.H. Mo, Y. Zhuang, X.B. Shen, Y. Xu, Q.Q. Lei, Q. Guo, Degradation characteristics of electron and proton irradiated InGaAsP/InGaAs dual junction solar cell, Sol. Energy Mater. Sol. Cells 206 (2020), 110339, https://doi.org/10.1016/j.solmat.2019.110339.

[18] C. Zhang, J. Zhang, Y. Hao, Z. Lin, C. Zhu, A simple and efficient solar cell parameter extraction method from a single current-voltage curve, J. Appl. Phys. 110 (2011), 064504, https://doi.org/10.1063/1.3632971.

[19] Y. Zhuang, A. Aierken, Q.Q. Lei, L. Fang, X.B. Shen, M. Heini, Q. Guo, J. Guo, X. Yang, J.H. Mo, R.K. Fan, J. Li, Q.Y. Chen, S.Y. Zhang, Optoelectronic performance analysis of low-energy proton irradiation and post-thermal annealing effects on InGaAs solar cell, Front. Physiol. 8 (2020), 585707, https://doi.org/10.3389/fphy.2020.585707.

[20] J. Li, A. Aierken, Y. Zhuang, P.Q. Xu, H.Q. Wu, Q.Y. Zhang, X.B. Wang, J.H. Mo, X. Yang, Q.Y. Chen, S.Y. Zhang, C.R. Yan, Y. Song, 1 MeV electron and 10 MeV proton irradiation effects on inverted metamorphic GaInP/GaAs/InGaAs triple junction solar cell, Sol. Energy Mater. Sol. Cells 224 (2021), 111022, https://doi.org/10.1016/j.solmat.2021.111022.

[21] M. Yamaguchi, S.J. Taylor, S. Matsuda, O. Kawasaki, Mechanism for the anomalous degradation of Si solar cells induced by high fluence 1 MeV electron irradiation, Appl. Phys. Lett. 68 (1996) 3141–3143, https://doi.org/10.1063/1.115804.

[22] N. Dharmarasu, M. Yamaguchi, A. Khan, T. Takamoto, T. Ohshima, H. Itoh, M. Imaizumi, S. Matsuda, Deep-level transient spectroscopy analysis of proton-irradiated n+/p InGaP solar cells, Phys. B Condens. Matter 308–310 (2001) 1181–1184, https://doi.org/10.1016/S0921-4526(01)00935-8.

[23] A. Johnston, Radiation damage of electronic and optoelectronic devices in space, present, 4th International Workshop on Radiation Effects on Semiconductor Devices for Space Application, Tsukuba, Japan (October 11-13, 2000).

[24] F. Chen, M. Zong, Z. Tan, X. Tang, Degradation characteristics and equivalent analysis of InGaAsP space solar cells under proton and neutron irradiation, Microelectron. Reliab. 151 (2023), 115249, https://doi.org/10.1016/j.microrel.2023.115249.

[25] T.B. Wang, Z.X. Wang, S.Y. Zhang, A. Aierken, B. Wang, L. Fang, Y. Zhuang, M. Li, G.H. Tang, Improved radiation resistance of flexible GaInP/GaAs dual junction solar cell by optimizing GaAs subcell i-layer, Mater. Sci. Semicond. Process. 163 (2023), 107562, https://doi.org/10.1016/j.mssp.2023.107562.

[26] X. Wang, B. Li, L. Zhou, X. Shi, L. Sun, X. Wang, Improving the irradiation resistance of inverted flexible 3J solar cells by adjusting the structure, Sol. Energy 249 (2023) 744–750, https://doi.org/10.1016/j.solener.2022.12.012.

[27] M. Zazoui, J.C. Bourgoin, Space degradation of multijunction solar cells: an electroluminescence study, Appl. Phys. Lett. 80 (2002) 4455–4457, https://doi.org/10.1063/1.1485134.

[28] D. Elfiky, M. Yamaguchi, T. Sasaki, T. Takamoto, C. Morioka, M. Imaizumi, T. Ohshima, S. Sato, M. Elnawawy, T. Eldesuky, A. Ghitas, Effect of base doping concentration on radiation-resistance for GaAs sub-cells in InGaP/GaAs/Ge, Jpn. J. Appl. Phys. 49 (2010), 121202, https://doi.org/10.1143/JJAP.49.121202.

[29] M.Q. Liu, S.Y. Zhang, T.B. Wang, Z.C. Tan, C.H. Du, C. Zeng, A. Aierken, Impacts of 14 MeV neutron irradiation on electrical and spectral properties of flexible GaInP/GaAs/InGaAs solar cells, Sol. Energy Mater. Sol. Cells 255 (2023), 112294, https://doi.org/10.1016/j.solmat.2023.112294.

[30] A. Aierken, Q. Guo, T. Huhtio, M. Sopanen, ChF. He, Y.D. Li, L. Wen, D.Y. Ren, Optical properties of electron beam and -ray irradiated InGaAs/GaAs quantum well and quantum dot structures, Radiat. Phys. Chem. 83 (2013) 42–47, https://doi.org/10.1016/j.radphyschem.2012.09.022.

[31] A.B. Dey, M.K. Sanyal, I. Farrer, K. Perumal, D.A. Ritchie, Q. Li, J. Wu, V. Dravid, Correlating photoluminescence and structural properties of uncapped and GaAs-capped epitaxial InGaAs quantum dots, Sci. Rep. 8 (2018) 7514, https://doi.org/10.1038/s41598-018-25841-7.

[32] D. Elfiky, M. Yamaguchi, T. Sasaki, T. Takamoto, C. Morioka, M. Imaizumi, T. Ohshima, S. Sato, M. Elnawawy, T. Eldesoky, A. Ghitas, Theoretical optimization of base doping concentration for radiation resistance of InGaP subcells of InGaP/GaAs/Ge based on minority-carrier lifetime, Jpn. J. Appl. Phys. 49 (2010), 121201, https://doi.org/10.1143/JJAP.49.121201.

[33] S.S. Li, W.L. Wang, R.Y. Loo, W.P. Rahilly, Study of deep-level defects and annealing effects in undoped and Sn-doped GaAs solar cells irradiated by one-MeV electrons, Solid State Electron. 26 (1983) 835–840, https://doi.org/10.1016/0038-1101(83)90053-9.